Electronic transport in GAA silicon nanowire MOSFETs: from Kubo-Greenwood mobility including screening remote coulomb scattering to analytical backscattering coefficient

J. Dura[1,2], F. Triozon[1], D. Munteanu[2], S. Barraud[1], S. Martinie[1], J.L. Autran[2]

[1] CEA-LETI MINATEC, 17 rue des Martyrs, 38054 Grenoble, Cedex 9, France
[2] IM2NP-CNRS, UMR CNRS 6242, Bât. IRPHE, 49 rue Joliot Curie, BP 146, 13384 Marseille Cedex 13, France
(e-mail : julien.dura@im2np.fr, Phone: +33 4 38 78 65 32, Fax:+33 4 38 78 51 40)

***Abstract*-- This paper presents the study of electron mobility in intrinsic silicon nanowires using the Kubo-Greenwood approach. This architecture (now considered as a realistic technology [1,2]) is aimed for ultra-scaled devices up to technology nodes sub-11nm [3] with silicon films of some nanometers. At these dimensions, the transport regime is completely modified due to the multi-subband transport. However, the promising potentialities of nanowires for microelectronic applications are not still demonstrated at all simulation levels (from atomistic to circuit performances). That is why the electronic transport is here investigated numerically using the Kubo-Greenwood approach coupled to a self-consistent Schrödinger-Poisson solver. Then, to support compact modelling including ultimate physical phenomena, an analytical model of the electron mobility and backscattering coefficient is exposed. The geometry dependence is essentially pointed out on the backscattering coefficient for a wide range of channel lengths (up to 10nm) and diameters (3nm≤Ø≤20nm).**

Keywords – **Nanowire MOSFET, modeling, electronic mobility, analytical backscattering coefficient.**

I. INTRODUCTION

Due to the exploration of alternative solutions featuring high performances, nanoelectronic devices have evolved towards architectures allowing a much better electrostatics control of the device active region compared to conventional MOSFETs. GAA nanowires MOSFETs, regarding their particular shape, are one of the most promising architectures. This is due to the surface controlled by the surrounding gate which is significantly much higher than for planar devices. With this architecture (now considered as a realistic technology due to recent significant progress of technological processes [1,2]), it is possible to envisage ultra-scaled devices as required by the International Technology Roadmap for Semiconductor (ITRS, [3]). In order to assess potentialities of such an architecture, a deep understanding is required from the electronic transport up to performances at the circuit level. Although theoretical papers already investigated nanowire transport, it is hardly to manage the physics up to circuit simulation. In this context, this paper focuses on the multi-subband electronic transport in nanowire for MOSFET application in order to provide brief analytical models to support simulation. In the following, we will concentrate on the electron mobility, and more particularly on the impact of diameter shrinking thanks to numerical investigation. Then, physics-based analytical model is provided up to the backscattering coefficient where the impact of diameter is assessed from a compact model point of view.

In the following, a cylindrical nanowire depicted in figure 1 is considered with a low-P-doped (10^{15}cm^{-3}) silicon channel delimited by highly N-doped source and drain regions. A High-κ/metal gate stack is used with a metal (Al) gate work function equal to 4.3eV.

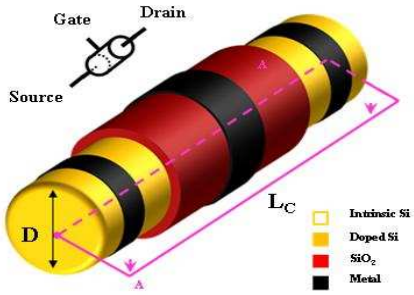

Fig. 1. Schematic of the GAA nanowire architecture and geometrical parameters definition.

II. KUBO-GREENWOOD INVESTIGATION FOR ELECTRON MOBILITY

The electronic structure is obtained computing a self-consistent Schrödinger-Poisson solver in cylindrical coordinates for a silicon nanowire oriented along the [001] axis. The 6 minima of the conduction band are described within the effective mass approximation. The 2 valleys along the [001] direction, named "longitudinal" valleys, have a confinement mass $m_t = 0.191m_e$ and a transport mass $m_l = 0.916m_e$, where m_e is the free electron mass. The 4 "transverse" valleys are anisotropic along the confinement directions. The cylindrical mass approximation is used here [4-6]: the confinement mass is $m_c = 2m_tm_l/(m_t+m_l)$ and the transport mass is m_t. This allows cylindrical symmetry to be used in the Schrödinger equation simplifying the system to one dimension. For thin nanowires (diameter < 5 nm), the effective mass approximation fails to describe accurately quantum confinement [6,7]. We modify the confinement masses given above in order to fit the energy levels given by a tight-binding calculation [8].

The mobility is computed in intrinsic cylindrical nanowires using the Kubo-Greenwood formula [9,10] based on the relaxation time approximation. Each

This work is partially founded by the IBM-STMicroelectronics-CEA/LETI-MINATEC Development Alliance.

interaction frequency is estimated using the Fermi golden rule based on the effective mass approximations corresponding to the probability to change from the initial state to the final one. The low-field electron mobility can be derived from the initial formula then modified to 1D transport [11] summing over the different valley α and subbands j:

$$\mu_{tot} = \frac{1}{n_{tot}} \sum_{\alpha j} n_{\alpha j} . \mu^{\alpha j} \quad (1)$$

where n_{tot} and $n_{\alpha j}$ are the total carrier concentration and the concentration in subband (α,j), respectively, and $\mu_{\alpha j}$ is the mobility of the subband expressed as:

$$\mu_{\alpha j} = \frac{2e}{kT.n_{\alpha j}.m_z^{\alpha}} \int_{E_{\alpha j}} g_{1D}^{\alpha j}(E).(E - E_{\alpha j}).\tau^{\alpha j}(E).f(E).(1 - f(E)).dE \quad (2)$$

where m_z^{α} is the effective mass of valley α, $E_{\alpha j}$ is the energy level of the subband j of the valley α, $f(E)$ is the Fermi-Dirac statistics, $g_{1D}^{\alpha j}$ is the density-of-states of the subband j and $\tau^{\alpha j}$ is the total momentum relaxation time. Main scattering mechanisms pointed out by experimental investigations are considered: phonons *ph*, surface roughness *SR* and remote coulomb scattering *RCS*. Scattering by ionized dopants is not included because nanowires are considered intrinsic. The total momentum relaxation time is obtained by summing the scattering rates of all mechanisms:

$$\frac{1}{\tau_{tot}^{\alpha j}} = \frac{1}{\tau_{ph}^{\alpha j}} + \frac{1}{\tau_{SR}^{\alpha j}} + \frac{1}{\tau_{RCS}^{\alpha j}} \quad (3)$$

Phonon and surface roughness scattering mechanism are given in accordance with the literature [4,11,12]. The last mechanism, *RCS*, due to trapped charges in the high-k/metal gate stack is investigated by solving the Poisson equation considering a local charge in the oxide.

The matrix element of the RCS perturbation induced by a single coulomb center of charge Q at the position r_c is defined by (α,j is the initial state and α',j' is the final state):

$$V_{\alpha j,\alpha' j'}^{c} = \frac{Q}{L_c.\varepsilon_{Si}} . \int_0^{\infty} \varphi_{\alpha j}.\varphi_{\alpha' j'}.G_{lq}(r, r_c).r.dr \quad (4)$$

where φ in the wave function, ε_{si} is the silicon permittivity, G is the Green function representing the dimensionless potential in the active region [6], l and q is the angular momentum and the wave vector difference between the initial and final state. The interest is so to us the angular dependence of the wave function even if only the radial part is used. The global matrix element of the system is easily obtained integrating the previous equation along all the trapped charge.

$$I_{\alpha j,\alpha' j'}^{c} = 2\pi.L_c . \int_0^{\infty} n_c(r_c) . \left| V_{\alpha j,\alpha' j'}^{c} \right|^2 . r_c . dr_c \quad (5)$$

where $n_c(r_c)$ is the coulomb center density along the radius axis of the nanowire.

The momentum relaxation time is obtained by injecting this matrix element in the Fermi golden rule:

$$\frac{1}{\tau_{RCS}} = \frac{L_c.\sqrt{2m^{\alpha}}}{\hbar^2} \sum_{\alpha' j'} \delta_{\alpha\alpha'} . I_{\alpha j,\alpha' j'}^{c} . \frac{\Theta(E - E_{\alpha j'})}{\sqrt{E - E_{\alpha j'}}} . \frac{1 + 2\beta[E - E_{\alpha j'}]}{\sqrt{E - E_{\alpha j'}}} \quad (6)$$

where β is the non-parabolic parameter.

The only term remaining to determine is $G_{lq}(r,r_c)$ which represents the normalized potential due to the charge localized in r_c with the retarded Green function satisfying the Poisson equation. Without screening effect, the Poisson equation in cylindrical coordinates is:

$$\left(\frac{\partial^2}{\partial r^2} + \frac{1}{r} . \frac{\partial}{\partial r} - q^2 - \frac{l^2}{r^2} \right) . G_{lq}(r, r_c) = \frac{\gamma}{r_c} . \delta(r - r_c) \quad (7)$$

with γ depends on the position of the charge (1 for a charge in the silicon film or $\varepsilon_{Si}/\varepsilon_{ox}$ for a charge in one of the gate oxide).

The system can be solved with the boundary conditions of the system. The solution and precisions about the resolution of the unscreened case is given in [6]. Then, screening effect due to the accumulated charge in the silicon film is considered using the Debye-Hückel approximation. In a previous work [6], we highlighted an expression for the screened Green $\tilde{G}$ potential as a correction.

$$\tilde{G}_{lq}(r) = G_{lq}(r, r_c) + \frac{\frac{S}{\pi} . G_{lq}(r, r_{max}) . G_{lq}(r_{max}, r_c)}{1 + \frac{S}{\pi} . G_{lq}(r_{max}, r_{max})} \quad (8)$$

where S is the screening parameter [6] and r_{max} is the maximum position of the wave function.

Main results are exposed in figure 2 with the green function with respect to position along the nanowire radius and the scattering rate due to trapped charge in the gate oxide. The result is that screening effect is not negligible as we can see figure 2 on the RCS interaction frequency of the first transverse subband.

III. ANALYTICAL MODEL OF MOBILITY

Finally, the total mobility including all scattering mechanisms is exposed and an analytical model reproducing the diameter dependence is developed inspired from master equations of the Kubo-Greenwood theory.

$$\mu_{total}^{-1} = \left(\frac{\mu_{0,ph}}{E^{\theta_{ph}}} \right)^{-1} + \left(\frac{\mu_{0,SR}}{E^{\theta_{SR}}} \right)^{-1} + \left(\frac{\mu_{0,RCS}}{E^{\theta_{RCS}}} \right)^{-1} \quad (9)$$

with

$$\begin{cases} \mu_{0,ph}(D) = \mu_{bulk,ph} . \sqrt{1 + A_{ph} . \delta D + B_{ph} . \delta D^4} \\ \mu_{0,SR}(D) = \mu_{bulk,SR} . \left(1 + A_{SR} . \delta D + B_{SR} . \delta D^4\right)^6 \\ \mu_{0,RCS}(D) = \frac{\mu_{bulk,RCS}}{N_{fix} . \pi . D} . \left(1 + A_{RCS} . \delta D + B_{RCS} . \delta D^4\right)^{3/2} \\ \delta D = \frac{D - D_{bulk}}{D_{bulk}} \end{cases} \quad (10)$$

where the parameters A, B and θ are fitting constants on numerical results, E is the effective transverse field and N_{fix} is the trapped charge density in the oxide.

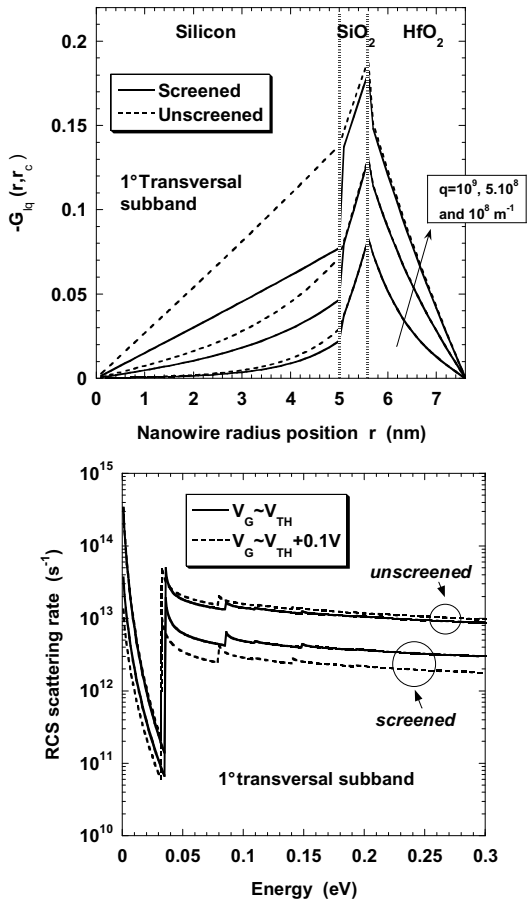

Fig. 2. Green function versus the position along the nanowire radius and for different wave vector (up); RCS interaction frequency for the first transversal subband for two different polarizations (around threshold voltage V_{TH} and 0.1V higher) (down). Comparison between the screened and unscreened cases.

Figure 3 shows the comparison between the analytical model and numerical results for the low-field electron mobility for the different scattering mechanisms as a function of the diameter (a), (b) and (c). Then, the total mobility is plotted with respect to the electron density in figure 4. We can note that the mobility is strongly impacted by the geometry for nanowire diameter less than 10nm.

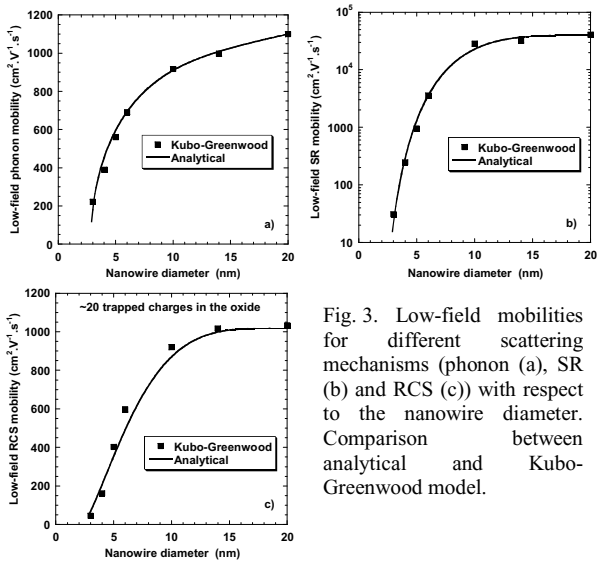

Fig. 3. Low-field mobilities for different scattering mechanisms (phonon (a), SR (b) and RCS (c)) with respect to the nanowire diameter. Comparison between analytical and Kubo-Greenwood model.

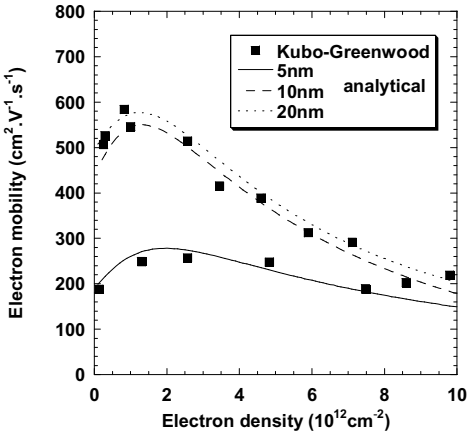

Fig. 4. Electron mobility as a function of the electron density for different nanowire diameters (5, 10 and 20nm). Comparison between analytical and Kubo-Greenwood model.

IV.ANALYTICAL BACKSCATTERING COEFFICIENT

The backscattering coefficient is the basis of the flux method initiated by McKelvey [13] and then developed by Natori/Lundstrom [14,15]. It defines the probability of carriers to be reflected back in the channel length by scattering and so the quality of the transport regime of the device as illustrated in figure 5.

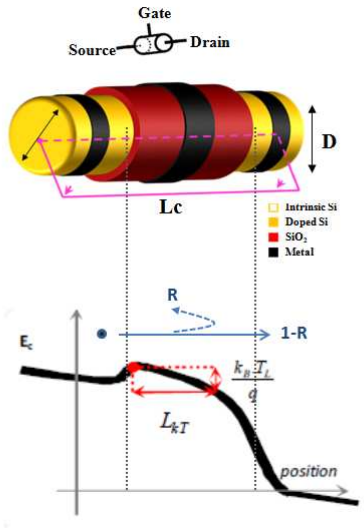

Fig. 5. Nanowire MOSFET schematics and energetic profile along the transport direction. Definition of the backscattering coefficient and the kT-layer.

In previous works, the backscattering coefficient R is described with a unified model valid for low and high electric field [13,16]. Two main concepts can be pointed out: the dynamical mean free path λ which is directly related to the mobility and the "kT-layer" L_{kT} which represents the impact of interactions on the energy barrier of the transistor. The "kT-layer" length [15] is modeled and validated on numerical simulations as shown in our previous work [17].

$$R = \frac{\lambda^{-1}}{\frac{1}{2}.L_{kT}^{-1}.\left(1+coth\left(\frac{1}{2}.\frac{L_c}{L_{kT}}\right)\right)+\lambda^{-1}} \quad (11)$$

with

$$\begin{cases} L_{kT} = L_c.\left(\frac{k.T}{q.V_{DS}}\right)^{1/\alpha} \\ \alpha = 1.9+\left(\frac{\lambda}{L_c}\right)^{0.7}.\frac{1.7}{1+e^{\frac{L_c-2D}{D}}} \\ \lambda = \frac{2.k.T}{q.v_{inj}}.\mu_{total} \end{cases} \quad (12)$$

where V_{DS} is the drain to source voltage and v_{inj} is the injection velocity.

However, in [17], bulk mobility was used without considering the effect of diameter. So, in this paper, R is computed introducing the analytical model of the mobility calibrated on Kubo-Greenwood results. Figure 6 plots the analytical backscattering coefficient versus the channel length for different diameters at low (charge equal to $10^{11}cm^{-2}$) and high (charge equal to $10^{13}cm^{-2}$) inversion regime. By reducing the channel length, we can note that the transport in the nanowire is improved toward a theoretical ballistic regime (R=0). However, reducing the diameter tends to limit the mobility (as we saw for Kubo-Greenwood results) and, as a consequence, the backscattering of carriers in the channel is higher. For high charge, the impact of the diameter seems to be attenuated.

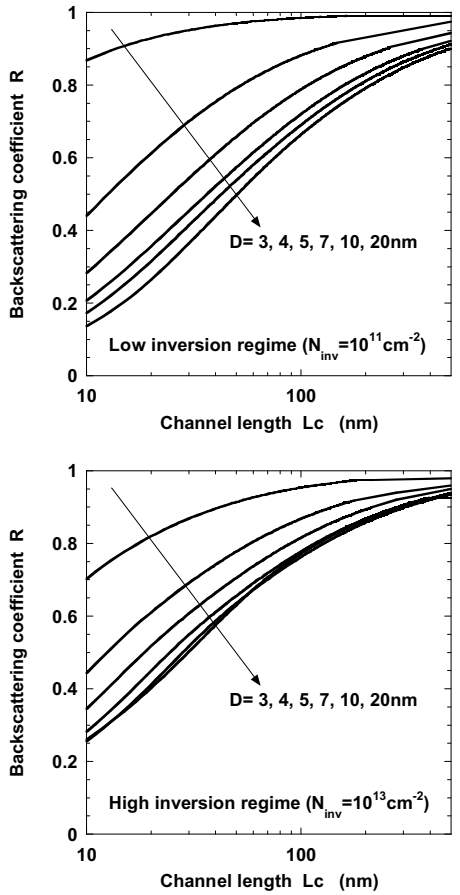

Fig. 6. Backscattering coefficient function of the channel length for different nanowire diameters (3, 4, 5, 7, 10 and 20nm) at low (a) and high (b) inversion regime.

V. CONCLUSION

A complete study of transport in silicon nanowire is performed from theoretical investigation with the use of the Kubo-Greenwwod formula up to the establishment of compact model for the mobility and the backscattering coefficient. Thanks to numerical results, the impact of diameters shrinking on the electron mobility has been highlighted. The main result is that a strong decrease is observed for diameter below 10nm which corresponds to dimensions recommended by the ITRS. This variation observed on the mobility must be included in compact model if we expect to provide predictive results even at circuit level. So, analytical expressions have been found out based on master equations of the Kubo-Greenwood theory to reproduce the diameter dependency. Then, in a previous work, we provided a unified compact model for the backscattering coefficient but based on bulk mobility. At the end of this paper, we included the analytical model of the mobility in this model to observe the impact of diameter on the backscattering coefficient in the different conduction regime (low and high inversion regimes).

REFERENCES

[1] K.H. Cho *et al*, *IEEE Electron Devices Letters*, vol. 28, no. 12, pp. 1129-1131, 2007.
[2] K. Tachi *et al.*, *IEDM Tech. Dig.*, pp.313-316, 2009.
[3] International Technology Roadmap for Semiconductors, 2011.
[4] S. Jin *et al*, J. Appl. Phys. 102, 083715 (2007).
[5] E. Gnani *et al*, IEEE Trans. Elec. Dev., vol. 54, 2243, 2007.
[6] J. Dura *et al*, J. Appl. Phys., vol. 111, 103710, 2012.
[7] A. Paussa *et al*, IEEE Trans. Elec. Dev ., vol. 57, 3239, 2010.
[8] J. Dura *et al*, Intech Open book, ISBN: 978-953-51-0239-7.
[9] R. Kubo, J. Phys. Soc. Jpn. 12, 570 (1957).
[10] D. A. Greenwood, Proc. Phys. Soc. London 71, 585 (1958).
[11] R. Kotlyar *et al*, Appl. Phys. Lett. 84, 5270 (2004).
[12] E. B. Ramayya *et al*, IEEE Trans. NanoTechnol. 6, 113 (2007).
[13] J.P. McKelvey *et al.*, *Physical Review,* vol. 123, no. 1, pp. 2736-2743, Jul. 1961.
[14] K. Natori *et al.*, *J. Appl. Phys.*, vol.76, no.8, pp.4879-4890, 1994.
[15] M. Lundstrom *et al*, *IEEE Trans. Electron Devices*, vol. 49, no. 1, pp. 131-141, Jan. 2002.
[16] S. Martinie *et al*, *IEEE Elect. Device Lett.*, vol. 29, no. 12, pp. 1392-1394, Dec. 2008.
[17] J. Dura *et al*, *IEEE Proc. SISPAD*, pp.43-46, 2011.